This is the pre-print of paper M. Milanese, L. Fagiano and D. Piga, "Control as a key technology for a radical innovation in wind energy generation," Proceedings of the 2010 American Control Conference, Baltimore, MD, 2010, pp. 2361-2377. doi: 10.1109/ACC.2010.5530562.

Control as a key technology for a radical innovation in wind energy generation

M. Milanese, L. Fagiano, D. Piga

***Abstract*— This paper is concerned with an innovative technology, denoted as Kitenergy, for the conversion of high-altitude wind energy into electricity. The research activities carried out in the last five years, including theoretical analyses, numerical simulations and experimental tests, indicate that Kitenergy could bring forth a revolution in wind energy generation, providing renewable energy in large quantities at lower cost than fossil energy. After an overview of the main features of the technology, this work investigates three important aspects: the evaluation of the performance achieved by the employed control law, the optimization of the generator operating cycle and the possibility to generate continuously a constant and maximal power output. These issues are tackled through the combined use of advanced modeling, control and optimization methods, which results to be key technologies for a significant breakthrough in renewable energy generation.**

I. Introduction

Sustainable energy generation is one of the most urgent challenges that mankind is facing today. Fossil sources (oil, gas, coal) cover at present about 80% of the global primary energy demand [1],[2], posing large problems, ranging from increasing fossil source costs (due to increasing energy demand in front of limited resources), to impact on climate change and on environment pollution, to geopolitical consequences of the fact that fossil sources are supplied by few producer countries. It is now widely recognized that a key strategy for facing these issues is a much more extensive use of renewable energy sources. This paper is focused on wind energy, which has large potentials. Wind industry has at present a value of about 30 billion $/year and, apart from hydropower plants, has the largest share of renewable energy generation, with yearly global growth of the installed capacity of about 30% in the last years, [3]. Indeed, by exploiting 20% only of the world land sites that are profitable for the actual wind technology, based on wind towers, the entire world's energy demand could be supplied [4]. However, the current wind technology has limitations in terms of energy production costs, which are still higher with respect to fossil sources, and in terms of land occupation, since wind farms based on modern wind towers of 2-3 MW rated power have an average power density of 3.5-4 MW/km^2 [5], about 200–300 times lower than that of large thermal plants. A comprehensive overview of the present wind technology is given in [6], where it is also pointed out that no big breakthrough is expected, but many evolutionary steps can cumulatively bring up to 30-40% improvements of cost effectiveness over the next decades. The main reason is that wind turbines operate at a maximum height of about 150 m over the ground, a value hardly improvable, due to structural constraints which have reached their technological limits. On the other hand, wind speed generally increases with height above the ground: at the height of 500–1000 meters the mean wind power density is about 4 times the one at 50–150 meters, and at 10,000 meters it is 40 times, [7]. This suggests that a breakthrough in wind energy generation can be realized by capturing wind power at altitudes over the ground that can not be reached by wind towers. The idea of harnessing high altitude wind power using a tethered aircraft has been proposed at least as far back as the 1970's, [8], [9], [10]. However, only in the past few years more intensive theoretical, technological and experimental studies have been carried out by academic research groups and/or high-tech companies, and many different High Altitude Wind (HAW) technologies have been proposed and investigated. These HAW technologies involve a large spectrum of different features and technical solutions, whose detailed presentation is not possible in this paper. Table I shows what are the main features of some of the proposed solutions, in terms of the following features:

- *Operating altitude over the ground* . The following ranges are mainly considered: 200-1000 meters, indicated as BL (Boundary Layer); 8,000-10,000 meters, indicated as JS (Jet Stream).
- *Lift type of the aircraft*. It can be distinguished as: AD (Aero-Dynamical lift, like the one exerted by airplane wings or kites); RC (Rotor-Craft lift, like that realized helicopters or autogyros); AS (Aero-Static lift like the one realized by lighter-than-air aircrafts).
- *Energy generation*. The energy can be generated: OB (On Board of the aircraft); GL (at the Ground Level).

TABLE I
FEATURES OF SOME HAW PROJECTS

Ref.	Altitude	Lift	Generation
T.U. Delft [11]	JS	AD	GL
T.U. Delft [12]	BL	AD	GL
Politecnico di Torino [13],[14],[15]	BL	AD	GL
K.U. Leuven [16]	BL	AD	GL
SkyWind Power[17]	JS	RC	OB
Magenn Power [18]	BL	AS	OB
Makani Power [19]	BL	AD	OB
Joby Energy [20]	JS	AD	OB
Skymill [21]	BL	RC	GL

HAW techniques for inland stationary electric energy generation only are considered in this paper and even for this

The authors are with Politecnico di Torino, Dipartimento di Automatica e Informatica, Corso Duca degli Abruzzi 24 - 10129 Torino - Italy

e-mail addresses: lorenzo.fagiano@polito.it, mario.milanese@polito.it, dario.piga@polito.it

This research was partly supported by funds of Regione Piemonte, Italy, under the Project "KiteNav: power kites for naval propulsion". Project partners: Politecnico di Torino, Azimut-Benetti s.p.a. and Modelway s.r.l.

case the above list is certainly not exhaustive. It must be noted that HAW techniques are being investigated also for naval propulsion, see e.g. [22], [23] and for offshore electric energy generation [24].

At Politecnico di Torino, starting from 2005, a HAW technology, indicated here as Kitenergy (KE), has been extensively investigated through modeling, computer simulation and experimental verification on a prototype, [13], [14], [15]. The main conclusion emerging from these studies is that KE technology, aimed to operate in the BL altitude range (in order to minimize the airspace occupation), has the potential of achieving energy generation costs lower than fossil energy and yearly generated energy per unit area of occupied land 10-20 times higher than that of the present wind technology. Thus, KE technology may represent a quantum leap in overcoming two main limitations of the present wind technology. These results can be obtained mainly thanks to the fact that energy is generated at the ground level and that the tethered wing flies in "crosswind", thus generating large aerodynamical lift forces. In this paper, the main modeling and control techniques of Kitenergy technology are outlined and some new results are presented on two configurations for energy generation, indicated as KE-yoyo and KE-carousel configurations.

II. Kitenergy technology

A. System description

The concept of Kitenergy is to use wings, linked to the ground by two cables, to extract energy from wind blowing at higher heights with respect to those of the actual wind technology. The flight of the wings is suitably driven by an automatic control unit. Wind energy is collected at ground level by converting the traction forces acting on the wing lines into electrical power, using suitable rotating mechanisms and electric generators placed on the ground. The wings are able to exploit wind flows at higher altitudes than those of wind towers (up to 1000 m, using 1200-1500-m-long cables), where stronger and more constant wind can be found basically everywhere in the world. This way, high-altitude wind energy can be harvested with the minimal effort in terms of generator structure, cost and land occupation. In the actual wind towers, the outermost 30% of the blade surface approximately contributes for 80% of the generated power. The main reason is that the blade tangential speed (and, consequently, the effective wind speed) is higher in the outer part, and wind power grows with the cube of the effective wind speed. Yet, the structure of a wind tower determines most of its cost and imposes a limit to the elevation that can be reached. To understand the concept of Kitenergy, one can imagine to remove all the bulky structure of a wind tower and just keep the outer part of the blades, which becomes a much lighter wing flying fast in crosswind conditions (see Fig. 1), connected to the ground by only the cables. Thus, the rotor and the tower of the present wind technology are replaced in Kitenergy technology by the wing and its cables, realizing a wind generator which is largely lighter and cheaper. For example, in a 2-MW wind turbine,

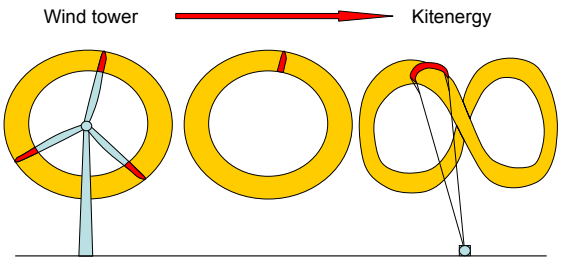

Fig. 1. Concept of Kitenergy technology

the weight of the rotor and the tower is typically about 300 tons (see [25]). As it will be shown in the next Sections, a Kitenergy generator of the same rated power can be obtained using a 500-m^2 wing and cables 1000-m long, with a total weight of about 2-3 tons only. The main components of a Kitenergy generator will be now briefly described.

The wing. High efficiency, maneuverability, resistance to strain and lightness are the main characteristics that a wing should have to be employed for high-altitude wind energy production. Aerodynamic efficiency is defined as the ratio between the lift and drag coefficients of the wing, denoted as C_L and C_D respectively. Such coefficients are functions of the attack angle α, i.e. the angle between the wing's longitudinal axis and the effective wind flow (see Fig. 2). Assuming an infinite wingspan, functions $C_L(\alpha)$ and $C_D(\alpha)$

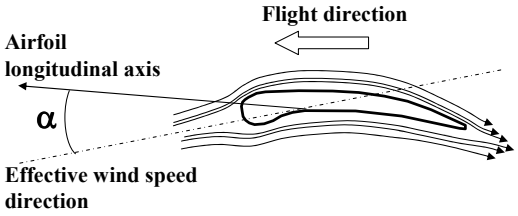

Fig. 2. wing during flight and attack angle α.

depends on the wing profile only. If a finite wingspan is considered, the effect of turbulence at the lateral edges of the wing reduces its aerodynamic efficiency. Such efficiency loss is higher with a lower aspect ratio, i.e. the ratio between the wing wingspan w_s and its chord c (Fig. 3(). Since at first

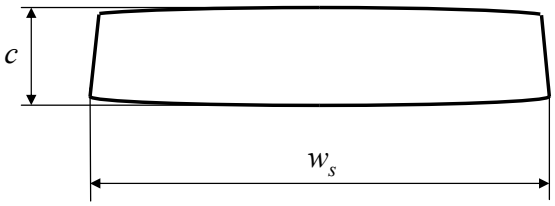

Fig. 3. wing top view: wingspan w_s and chord c.

approximation the generated power increases with the square of aerodynamic efficiency, wings with high aspect ratios (i.e. high wingspan) should be employed. The maneuverability of the wing, in terms of minimal turning radius R_F during

the flight, also depends on its wingspan, according to the approximate relationship:

$$R_F \simeq 2.5\, w_s. \tag{1}$$

Since the optimal wing trajectory is a loop or a "figure eight" in the air (see [16]), its wingspan should be contained in order to obtain trajectories that are as strict as possible, thus allowing to make more wings operate close one to the other in a relatively small area. Thus, efficiency and maneuverability lead to opposite requirements on the wing geometry. As regards resistance and lightness, such characteristics depend mainly on the employed material and partly on the wing design. Flexible materials and air-inflated structures have been employed so far in the development of Kitenergy, since they are light and cheap and provide sufficient rigidity. In particular, commercially available power kites used for surfing or sailing have been employed, so that in the following the wing will be also referred to as "kite". Such power kites are not designed for generating energy and therefore their efficiency is relatively low. Indeed, rigid wings made of innovative composite materials and designed to maximize efficiency could provide a noticeable performance improvement.

The cables. The wing lift force is converted into mechanical power through the traction forces acting on the lines. Thus, the latter have to be strong enough to support high loads. At the same time, the cables have to be light and their diameter should be kept as small as possible, to limit their weight and aerodynamic drag. Lines realized in composite materials, with a traction resistance 8-10 times higher than that of steel cables of the same weight, are being employed in the Kitenergy project. In order to extract energy from wind flows between 200-1000 m of elevation, 500-1500-m-long lines are needed. The prototype built in the Kitenergy project is equipped with two 1000-m cables and has already reached the target height of 800 m above the ground.

The Kite Steering Unit (KSU). At ground level, the two wing cables are rolled by winches linked to electric drives which are able to act either as generators or as motors. The kite flight is tracked using on-board wireless instrumentation (GPS, magnetic and inertial sensors) as well as ground sensors, to measure the wing speed and position, the power output, the cable force and speed and the wind speed and direction. Such variables are employed for feedback by a control system, able to influence the kite flight by differentially pulling the cables, via a suitable control of the electric drives. The system composed by the electric drives, the drums, the on-board sensors and all the hardware needed to control a single kite is denoted as Kite Steering Unit (KSU) and it is the core of the Kitenergy technology (see Fig. 4, where a picture of the KSU prototype realized at Politecnico di Torino is shown). The KSU can be employed in different ways to generate energy, depending on how the traction forces acting on the cables are converted into mechanical and electrical power. In particular, two different configurations have been investigated so far, namely the KE-yoyo and the KE-carousel configurations. In the KE-yoyo configuration, the KSU is fixed on the ground and wind power is captured by unrolling the kite lines, while in the KE-carousel configuration the KSU is put on a vehicle pulled by the lines along a circular path, thus generating energy by means of additional electric generators linked to the wheels. In the following, the operating cycles of the KE-yoyo and KE-carousel generators will be described. Indeed, these high-altitude wind energy generators are complex, open-loop unstable systems, affected by external disturbances (e.g. wind turbulence), with nonlinear dynamics and operational constraints. Thus, the use of advanced automatic control techniques, able to stabilize the kite flight while coping with disturbances and constraints, is the crucial feature of Kitenergy, since it is fundamental to achieve the best energy generation performance, as it will be highlighted in Section III-B.

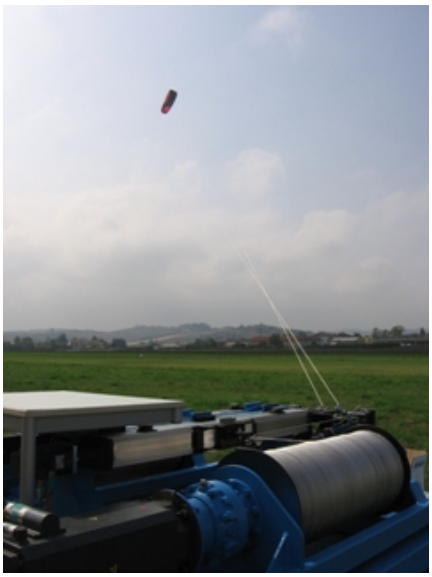

Fig. 4. Kite Steering Unit (KSU) small-scale prototype operating near Torino, Italy.

B. Kitenergy configurations and operating cycles

KE-yoyo configuration. In the KE-yoyo configuration, the KSU is fixed with respect to the ground. Energy is obtained by continuously performing a two-phase cycle (depicted in Fig. 5): in the *traction phase* the controller is designed in such a way that the kite unroll the lines, maximizing the power generated by the electric drives that are driven by the rotation of the drums. When the maximum line length is reached, the *passive phase* begins and the drives act as motors, spending a minimum amount of the previously generated energy, to recover the kite and to drive it in a position which is suitable to start another traction phase. The

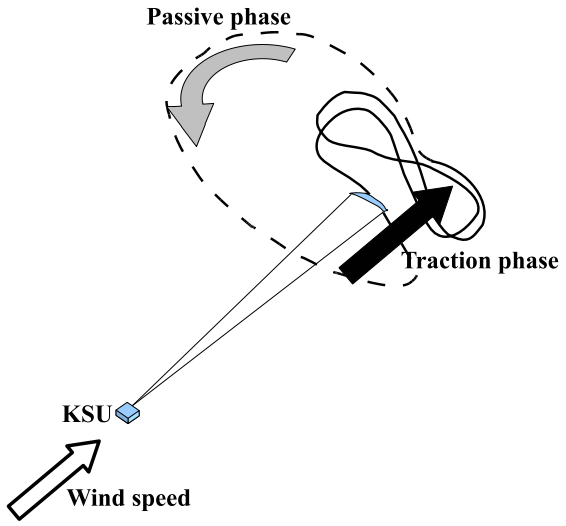

Fig. 5. Sketch of a KE-yoyo cycle: traction (solid) and passive (dashed) phases.

passive phase can be performed in two possible ways (see Fig. 6):

I) **"low power maneuver"**: the kite is driven to the borders of the "power zone" (see Fig. 6), where the effective wind speed (and, consequently, the aerodynamic lift force) drops to low values thus allowing to recover the cables with low energy expense;

II) **"low lift maneuver"**: by using additional actuators onboard of the wing, the attack angle are modified in order to make the kite lose its aerodynamic lift and to allow a fast winding back of the cables with low energy losses.

The low lift maneuver has the advantage of occupying less aerial space than the low power maneuver, however it requires additional actuators on the kite. For the whole KE-

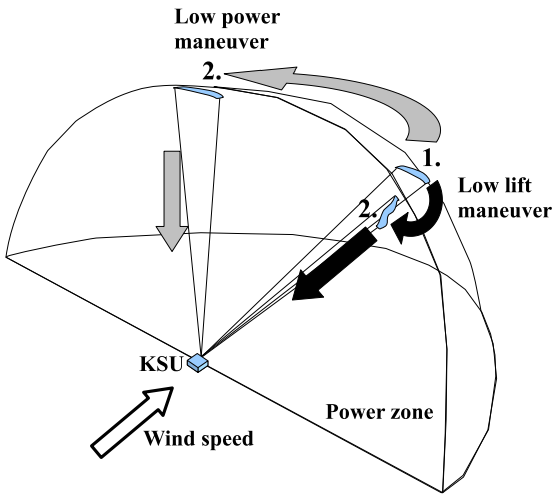

Fig. 6. KE-yoyo passive phase: "low power" (gray) and "low lift" (black) maneuvers.

yoyo cycle to be generative, the total amount of energy produced in the traction phase has to be greater than the energy spent in the passive one. Therefore, the controller employed in the traction phase must maximize the produced energy, while in the passive phase the objective is to maneuver the kite in a suitable way to minimize, at the same time, the spent energy (see e.g. [14] for details).

KE-carousel configuration. In a KE-carousel, the KSU is placed on a vehicle moving along a circular path (see Fig. 7); the vehicle wheels are connected to electric drives, which can generate electric energy and, suitably controlled, can also regulate the vehicle speed.

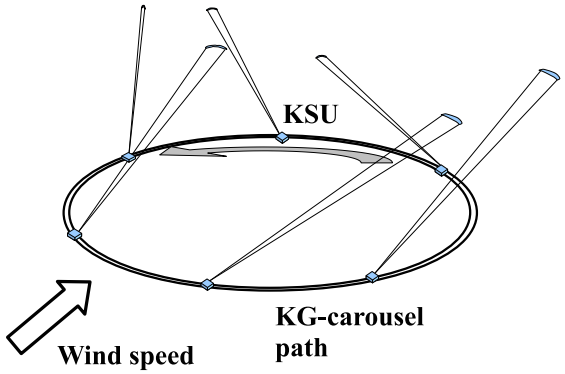

Fig. 7. Sketch of a KE-carousel.

The potentials of the KE-carousel configuration have been investigated using either variable line length or constant line length.

I) **Constant line length**. When a fixed cable length is employed, energy is generated by continuously repeating a cycle composed of two phases, namely the *traction* and the *passive* phases. These phases are related to the angular position Θ of the control unit, with respect to the wind direction (see Fig. 8). During the traction phase, which begins at $\Theta =$

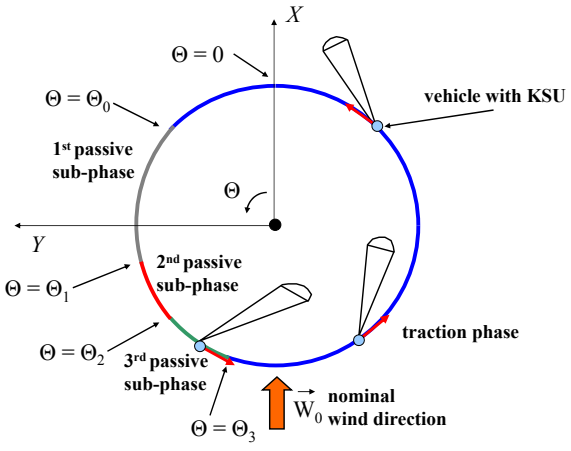

Fig. 8. KE-carousel configuration phases with constant line length.

Θ_3 in Fig. 8, the controller is designed in such a way that the kite pulls the vehicle, maximizing

the generated power. This phase ends at $\Theta = \Theta_0$ and the passive phase begins: the kite is no more able to generate energy until angle Θ reaches the value Θ_3. In the passive phase, the controller is designed to move the kite, with the minimal energy loss, in a suitable position to begin another traction phase, where once again the control is designed to maximize the generated power (see e.g. [13], [26] for details).

II) **Variable line length**. If line rolling/unrolling is suitably managed during the cycle, energy can be generated also when the vehicle is moving against the wind. In this case the operating phases, namely the *traction* and the *unroll* phases, are depicted in Fig. 9. The *unroll phase* approximately begins

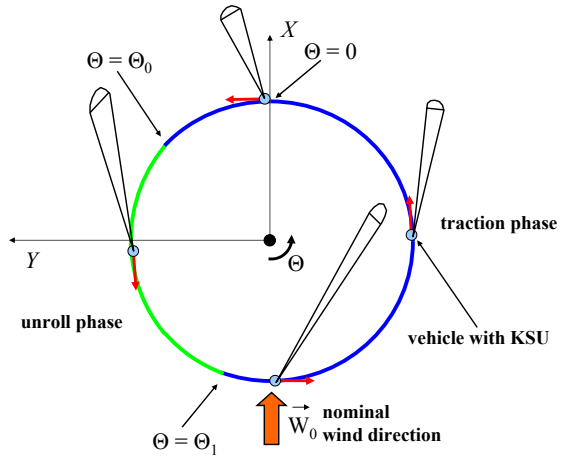

Fig. 9. KE-carousel configuration phases with variable line length.

when the angular position Θ of the vehicle is such that the KSU is moving in the opposite direction with respect to the nominal wind: such situation is identified by angle Θ_0 in Fig. 9. During the unroll phase, the electric drives linked to the vehicle wheels act as motors to drag the KSU against the wind. At the same time, the kite lines unroll, thus energy is generated as in the traction phase of the KE-yoyo configuration. The difference between the energy spent to drag the vehicle and the energy generated by unrolling the lines gives the net energy generated during this phase. When the KSU starts moving with wind advantage (i.e. its angular position is greater than Θ_1 in 9), the KE-carousel *traction phase* starts: the kite pulls the vehicle and the drives linked to the wheels act as generators. Meanwhile, the kite lines are rolled back in order to always start the next unroll phase with the same line length. Thus, in the traction phase the net generated energy is given by the difference between the energy generated by pulling the vehicle and the energy spent to recover the lines. Therefore, the controller employed in the KE-carousel with variable line length has to be designed in order to maximize such a net generated energy. The control design and simulation results of a KE-yoyo carousel with variable line length have been presented in [14], considering a fixed speed of the KSU along the carousel path. As a matter of fact, a variable vehicle speed can be exploited in the KE-carousel as an additional degree of freedom: in this paper, this possibility is investigated and compared with the KE-yoyo and KE-carousel with constant line length (see Sections IV-C and VI)

III. Modeling and Control of Kitenergy

A. System model

The mathematical models of the described Kitenergy generators will be now briefly resumed. For more details on the system model, the interested reader is referred to [14], [15], [26].

A fixed Cartesian coordinate system (X, Y, Z) is considered (see. Fig. 11(b)), with X axis aligned with the nominal wind speed vector direction. Wind speed vector is represented as $\vec{W}_l = \vec{W}_0 + \vec{W}_t$, where $\vec{W}_0$ is the nominal wind, supposed to be known and expressed in (X, Y, Z) as:

$$\vec{W}_0 = \begin{pmatrix} W_x(Z) \\ 0 \\ 0 \end{pmatrix} \tag{2}$$

$W_x(Z)$ is a known function which gives the wind nominal speed at the altitude Z. The term $\vec{W}_t$ may have components in all directions and is not supposed to be known, accounting for wind unmeasured turbulence. In the performed studies, function $W_x(Z)$ corresponds to a wind shear model (see e.g. [4]):

$$W_x(Z) = W_0 \frac{\ln\left(\frac{Z}{Z_r}\right)}{\ln\left(\frac{Z_0}{Z_r}\right)}, \tag{3}$$

where W_0, Z_0 and Z_r are the wind shear model parameters. An example of wind shear profile related to the site of Brindisi, Italy, during winter months is reported in Fig. 10, where the parameters have been estimated as $W_0 = 7.4\,\text{m/s}$, $Z_0 = 32.5\,\text{m}$ and $Z_r = 6\,10^{-4}\,\text{m}$ using the data contained in the database RAOB (RAwinsonde OBservation) of the National Oceanographic and Atmospheric Administration, see [27].

A second, possibly moving, Cartesian coordinate system (X', Y', Z') is considered, centered at the Kite Steering Unit (KSU) location. In this system, the kite position can be expressed as a function of its distance r from the origin and of the two angles θ and ϕ, as depicted in Fig. 11(a), which also shows the three unit vectors e_θ, e_ϕ and e_r of a local coordinate system centered at the kite center of gravity. In the KE-carousel configuration, the KSU angular position Θ is defined by the direction of X and X' axes (see Fig. 11(b)).

Applying Newton's laws of motion to the kite in the local

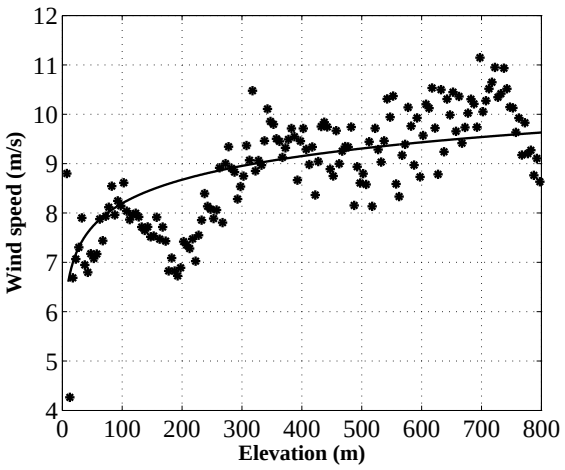

Fig. 10. Wind shear model, related to the site of Brindisi (Italy) during winter months, employed in the simulation of the optimized KE-yoyo with low lift recovery maneuver.

coordinate system $(e_\theta,\, e_\phi,\, e_r)$, the following dynamic equations are obtained:

$$\begin{aligned} \ddot{\theta} &= \frac{F_\theta}{m\, r} \\ \ddot{\phi} &= \frac{F_\phi}{m\, r \sin\theta} \\ \ddot{r} &= \frac{F_r}{m} \end{aligned} \tag{4}$$

where m is the kite mass. Forces F_θ, F_ϕ and F_r include the contributions of gravity force $\vec{F}^{\text{grav}}$ of the kite and the lines, apparent force $\vec{F}^{\text{app}}$, kite aerodynamic force $\vec{F}^{\text{aer}}$, aerodynamic drag force $\vec{F}^{\text{c,aer}}$ of the lines and traction force $F^{\text{c,trc}}$ exerted by the lines on the kite.

Gravity forces take into account the kite weight and the contribution given by the weight of the lines. Apparent forces include centrifugal and inertial forces due to the kite and KSU movement. The kite aerodynamic force $\vec{F}^{\text{aer}}$ can be derived via the computation of the lift and drag forces, $\vec{F}_L$ and $\vec{F}_D$ respectively, that depend on the air density ρ, on the kite effective wind speed $\vec{W}_e$, on the kite area A, on the kite aerodynamic lift and drag coefficients, C_L and C_D respectively, which in turn depend on the kite attack angle α (see [14] for more details):

$$\begin{aligned} \vec{F}_L &= -\frac{1}{2}\, C_L\, A\, \rho\, |\vec{W}_e|^2\, \vec{z}_{\text{w}} \\ \vec{F}_D &= \frac{1}{2}\, C_L\, A\, \rho\, |\vec{W}_e|\, \vec{W}_e \end{aligned} \quad . \tag{5}$$

In (5), the unit vector $\vec{z}_{\text{w}}$ is perpendicular to the effective wind speed $\vec{W}_e$ and points down when $\vec{W}_e$ is parallel to the ground. The control variable is the angle ψ, that can influence the roll angle of the kite, thus changing the orientation of the unit vector $\vec{z}_{\text{w}}$. Angle ψ is defined as:

$$\psi \doteq \arcsin\left(\frac{\Delta l}{d}\right), \tag{6}$$

with d being the distance between the two lines fixing points at the kite and Δl the length difference of the two lines,

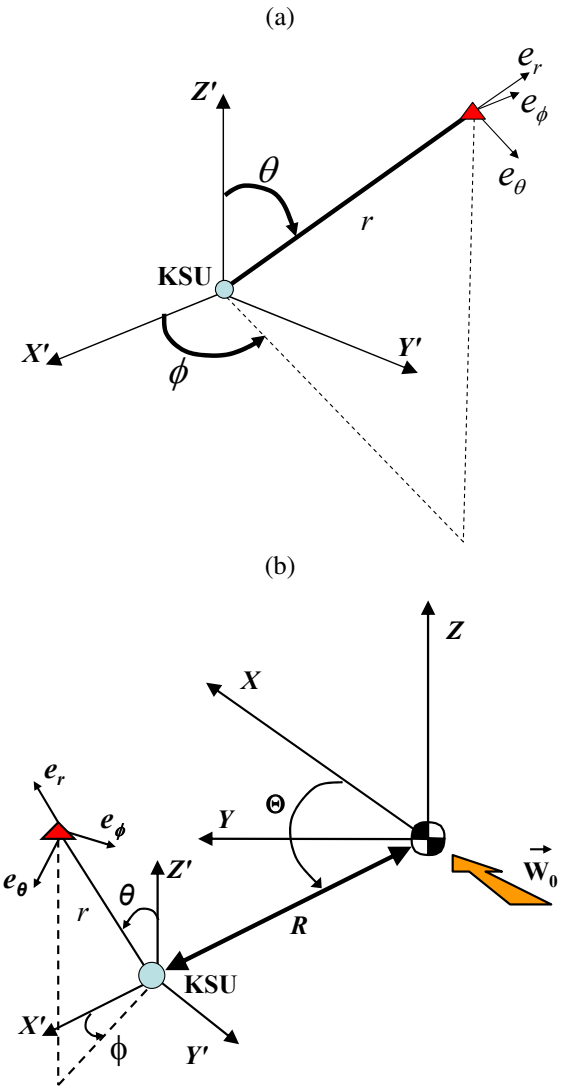

Fig. 11. (a) Model diagram of a single KSU (b) Model diagram of a single KSU moving on a KE-carousel.

which can be issued by a suitable control of the electric drives. Finally, the influence of the lines is taken into account in the model through their drag force $\vec{F}^{\text{c,aer}}$ and the traction force $F^{\text{c,trc}}$. $\vec{F}^{\text{c,aer}}$ depends on the line drag coefficient $C_{D,l}$, on the line length r and diameter d_l. The traction force $F^{\text{c,trc}}$ is always directed along the local unit vector e_r and cannot be negative, since the kite can only pull the lines. Moreover, $F^{\text{c,trc}}$ is measured by a force transducer on the KSU and, using a local controller of the electric drives, it is regulated in such a way that $\dot{r}(t) = \dot{r}_{\text{ref}}$ where $\dot{r}_{\text{ref}}$ is a reference line rolling speed.

In the case of KE-carousel configuration, the motion law of the KSU along the circular path of radius R has to be included too, with the following equation:

$$M\ddot{\Theta}R = F^{\text{c,trc}} \sin\theta \sin\phi - F^{\text{gen}} \tag{7}$$

where M is the total mass of the vehicle and the KSU and F^{gen} is the force exerted by the electric drives linked to

the wheels. It is supposed that suitable kinematic constraints (e.g. s) oppose to the centrifugal inertial force acting on the vehicle and to all the components of the line force, except for the one acting along the tangent to the vehicle path (i.e. $F^{\text{c,trc}} \sin\theta \sin\phi$). Note that any viscous term is neglected in equation (7), since the vehicle speed $\dot{\Theta}R$ is kept very low as it will be shown in Section V. F^{gen} is positive when the kite is pulling the vehicle toward increasing Θ values, thus generating energy, and it is negative when the electric drives are acting as motors to drag the vehicle against the wind, when the kite is not able to generate a suitable pulling force. Considering that the kite altitude Z depends on r and θ:

$$Z = r\cos(\theta), \tag{8}$$

the model equations (2)-(8) give the system dynamics in the form:

$$\dot{x}(t) = f(x(t), u(t), \dot{r}_{\text{ref}}(t), \dot{\Theta}_{\text{ref}}(t), \alpha, \vec{W}_t(t)) \tag{9}$$

where $x(t) = [\theta(t)\ \phi(t)\ r(t)\ \Theta(t)\ \dot{\theta}(t)\ \dot{\phi}(t)\ \dot{r}(t)\ \dot{\Theta}(t)]^T$ are the model states and $u(t) = \psi(t)$ is the control input. Clearly, in the case of KE-yoyo configuration $\Theta = \dot{\Theta} = \dot{\Theta}_{\text{ref}} = 0$. The net mechanical power P generated (or spent) is the algebraic sum of the power generated (or spent) by unrolling/recovering the lines and by the vehicle movement:

$$P(t) = \dot{r}(t) F^{\text{c,trc}}(t) + \dot{\Theta}(t)\, R\, F^{\text{gen}}(t) \tag{10}$$

For the KE-yoyo configuration the term $\dot{\Theta}\, R\, F^{\text{gen}} = 0$ and generated mechanical power is only due to line unrolling.

Note that in all the paper the aim is to evaluate the mechanical power that can be obtained, without considering the problem of how to transform in the most efficient way this mechanical power in electric power.

B. Control requirements and controller design

Advanced control techniques are fundamental to operate high-altitude power generators. In fact, the kite flight has to be stabilized and suitably controlled to continuously perform the different operational phases of the KE-yoyo or KE-carousel configurations. In each of the working phases, the objective to be achieved can be formulated as an optimization problem with its own cost function and with state and input constraints, in order to prevent the kite from getting too close to the ground and to avoid line wrapping and interference among more kites flying close in the same area. Then, a suitable control strategy has to be employed, able to achieve the required objective while avoiding constraint violation. To this end, Nonlinear Model Predictive Control (NMPC, see e.g. [28]) techniques are employed, since they are able to take into account state and input constraints.

In NMPC, the control move computation is performed using a discrete time model derived from the above continuous state equations on the basis of a suitably chosen sampling period Δ_t. At each sampling time $t_k = k\Delta_t$, $k \in \mathbb{N}$, the measured values of the state $x(t_k)$ and of the angle Θ are used to compute the control move through the optimization of a performance index of the form:

$$J(U, x(t_k), \dot{r}_{\text{ref}}, \dot{\Theta}_{\text{ref}}) = \int_{t_k}^{t_k+T_p} L(\tilde{x}(\tau), \tilde{u}(\tau), \Theta) d\tau \tag{11}$$

where $T_p = N_p\Delta_t$, $N_p \in \mathbb{N}$ is the prediction horizon, $\tilde{x}(\tau)$ is the state predicted inside the prediction horizon according to the state equation (16), using $\tilde{x}(t_k) = x(t_k)$ and the piecewise constant control input $\tilde{u}(t)$ belonging to the sequence $U = \{\tilde{u}(t)\}$, $t \in [t_k, t_{k+T_p}]$ defined as:

$$\tilde{u}(t) = \begin{cases} \bar{u}_i,\ \forall t \in [t_i, t_{i+1}],\ i = k, \ldots, k+T_c-1 \\ \bar{u}_{k+T_c-1},\ \forall t \in [t_i, t_{i+1}],\ i = k+T_c, \ldots, k+T_p-1 \end{cases} \tag{12}$$

where $T_c = N_c\Delta_t$, $N_c \in \mathbb{N}$, $N_c \leq N_p$ is the control horizon.

The cost $L(\cdot)$ in (11) is suitably defined on the basis of the performances to be achieved. In the considered problem, function $L(\cdot)$ is designed according to the operational phase of the generator (i.e. traction and passive phases for the KE-yoyo and fixed-line KE-carousel or traction and unroll phases for the variable-line KE-carousel, see Section II-B). Details on the choices of the cost function can be found in [13], [14], [26]. Moreover, in order to take into account the existing physical limitations on both the kite flight and the control input ψ, constraints of the form $\tilde{x}(t) \in \mathbb{X}$, $\tilde{u}(t) \in \mathbb{U}$ have been included too. In particular, the following state constraint is considered to keep the kite sufficiently far from the ground:

$$\theta(t) \leq \overline{\theta} \tag{13}$$

with $\overline{\theta} < \pi/2$ rad. Actuator physical limitations give rise to the constraints:

$$\begin{aligned} |\psi(t)| &\leq \overline{\psi} \\ |\dot{\psi}(t)| &\leq \overline{\dot{\psi}} \end{aligned} \tag{14}$$

As a matter of fact, other technical constraints have been added to force the kite to go along "figure eight" trajectories rather than circular ones, in order to prevent the lines from wrapping one around the other.

The predictive control law is then computed using a receding horizon strategy, in which the following nonlinear program has to be solved at each sampling time:

$$\min_{U} \quad J(U, x(t_k), \dot{r}_{\text{ref}}, \dot{\Theta}_{\text{ref}}) \tag{15a}$$

$$\text{subject to} \tag{15b}$$

$$\tilde{x}(t_k) = x(t_k) \tag{15c}$$

$$\dot{\tilde{x}}(t) = f(\tilde{x}(t), \tilde{u}(t), \dot{r}_{\text{ref}}(t), \dot{\Theta}_{\text{ref}}(t), W_x(t))\ \forall t \in (t_k, t_{k+T_p}] \tag{15d}$$

$$\tilde{x}(t) \in \mathbb{X},\ \tilde{u}(t) \in \mathbb{U}\ \forall t \in [t_k, t_{k+T_p}] \tag{15e}$$

The predictive controller results to be a nonlinear static function of the system state x and the reference speed values $\dot{r}_{\text{ref}}$, $\dot{\Theta}_{\text{ref}}$ imposed to the local drive controllers of the KSU and of the carousel vehicle (see Section III-A):

$$u(t_k) = \kappa(x(t_k), W_x(t_k), \dot{r}_{\text{ref}}(t_k), \alpha(t_k), \dot{\Theta}_{\text{ref}}(t_k)) \tag{16}$$

An efficient NMPC implementation is needed in Kitenergy for the real time control computations, since a sampling time of the order of 0.2 sec. is required. To this end, the fast implementation technique of the obtained predictive controller presented in [29] is adopted. Finally, the system state

needed by the control algorithm can be reliably measured or estimated through advanced direct filtering and sensor fusion techniques (see e.g. [30]).
Simulation results obtained by the described control strategy are presented in [14], [15] and show that the NMPC control laws are very effective, giving a generated power of up to 10 MW with a single KSU unit equipped with a 500 m^2 kite with an aerodynamic efficiency of 8-10 and wind speed of 15 m/s. These studies allow to estimate that wind farms based on KE technology can have energy generation costs significantly lower than from fossil sources, as shown in Table (II) (reported from [15]), where a comparison is made with the costs of other energy generation technologies as evaluated in [31]. Moreover, the first experimental results

TABLE II

PROJECTED COST IN 2030 (LEVELISED IN 2003 U.S. DOLLARS PER MWH) OF ENERGY FROM DIFFERENT SOURCES, COMPARED WITH THE ESTIMATED ENERGY COST OF KITEENERGY.

Source	Minimal estimated ($/MWh)	Maximal estimated ($/MWh)	Average estimated ($/MWh)
Coal	25	50	34
Gas	37	60	47
Nuclear	21	31	29
Wind	35	95	57
Solar	180	500	325
KiteEnergy	10	48	20

obtained with a small-scale prototype (see Fig. 4 and the movies [32], [33]) show a good matching with the employed model, thus increasing the confidence in the above-reported cost estimates, see [14], [15] for details.
In this paper, we investigate some further questions arising in the control design of KE technology:

- In each phase, the NMPC approach requires the solution of the optimization problem (15) which, being the model nonlinear, may be not convex, and the numerical optimization algorithm may be trapped in local minima. Moreover, in order to limit the computational complexity, the prediction horizon T_p in (11) is much shorter than the duration of the generator cycle. Thus, it is important to evaluate how far the obtained performance is from optimality.
- The overall control strategy requires to design not only the control law $u(t_k)$, but also several "operational" parameters (e.g. $\dot{r}_{\text{ref}}, \alpha, \dot{\Theta}_{\text{ref}}$,..), that have to be set up according to the wind speed, wing's and cable features, etc., in order to maximize the generated energy over the whole generation cycle.
- In the KE-yoyo and in the constant-length KE-carousel configurations, the energy generation is not constant, due to the periodic cycling between traction and passive phases. It is of interest to evaluate if it is possible to have a KE-carousel configuration that does not require passive phases, so that the energy production is constant and possibly maximal.

The key idea for answering these questions is to employ simplified equations, giving the generated power as a function of all of the main involved operational parameters and variables, together with optimization techniques, to derive the operating conditions that achieve the maximal generated power. Indeed, such equations are based on simplified hypotheses (for example inertial forces are neglected, see below), which in general lead to higher power values than the ones derived by the much more detailed model described in Section III-A. Indeed, as shown in the following, such overbounding is quite moderate. As an original contribution of this paper, such a procedure is applied to evaluate whether in each phase the NMPC strategy is able to achieve optimal energy generation performance, and to optimally design the operational cycles of a KE-yoyo and of a KE-carousel with either fixed or variable line length. Then, numerical simulations using the optimized parameters will be carried out in Section V, in order to assess the matching between the results obtained by the simplified equations and by the dynamical model (9).

C. Simplified equations of kite power

Consider a wing linked by a cable to a point at ground level (i.e. the KSU). Indicate with r the cable length and with $\vec{e}_r$ a unit vector parallel to the cable and pointing towards increasing r values (see Fig. 12). Moreover, indicate with $\vec{W}_e$ the effective wind speed, i.e. the vector sum of absolute wind speed and of the wing speed with respect to the ground, and with $\vec{W}_{e,p}$ the projection of $\vec{W}_e$ on the plane perpendicular to vector $\vec{e}_r$. The magnitudes of the wing lift and drag forces,

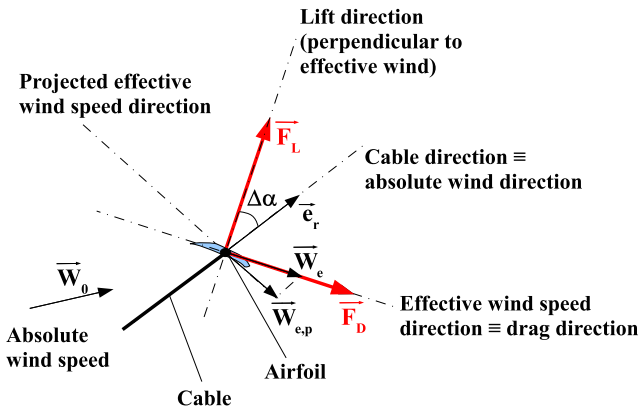

Fig. 12. Sketch of a wing flying in crosswind conditions.

$|\vec{F}_L|$ and $|\vec{F}_D|$ respectively, can be computed as (see 5):

$$\begin{aligned} |\vec{F}_L| &= \frac{1}{2}\rho A C_L |\vec{W}_e|^2 \\ |\vec{F}_D| &= \frac{1}{2}\rho A C_D |\vec{W}_e|^2 \end{aligned} \tag{17}$$

where ρ is the air density, C_L and C_D are the lift and drag aerodynamic coefficients and A is the wing projected area. Assume that:

- the kite flies in crosswind conditions;

- the inertial and apparent forces are negligible with respect to the aerodynamic forces;
- the kite speed relative to the ground is constant;
- the kite speed relative to the ground is much higher than the speed of the KSU relative to the ground;
- the kite aerodynamic lift force $\vec{F}_L$ approximately lies on the plane defined by vectors $\vec{W}_{e,p}$ and $\vec{e}_r$.

Then, it can be shown that the total traction force $F^{\text{c,trc}}$ acting on the cables can be computed as (see e.g. [10], [34], [35]):

$$F^{\text{c,trc}} = C|\vec{W}_{e,r}|^2 \tag{18}$$

where

$$\begin{aligned} C &= \frac{1}{2}\rho A C_L E_{\text{eq}}^2 \left(1 + \frac{1}{E_{\text{eq}}^2}\right)^{\frac{3}{2}} \\ E_{\text{eq}} &= \frac{C_L}{C_D\left(1 + \frac{(2\,r\,d_l)\,C_{D,l}}{4\,A\,C_D}\right)} \end{aligned} \tag{19}$$

and $|\vec{W}_{e,r}|$ is the magnitude of projection of the effective wind speed on the cable direction, computable as:

$$|\vec{W}_{e,r}| = \left||\vec{W}_0|\sin(\theta)\cos(\phi+\Theta) - \dot{r} - R\dot{\Theta}\sin(\phi)\right|. \tag{20}$$

Then, the generated power can be obtained by combining equations (10) and (18):

$$P(t) = \dot{r}(t)F^{\text{c,trc}} + \dot{\Theta}\,R\,F^{\text{c,trc}}\sin(\theta)\sin(\phi) \tag{21}$$

Note that equation (18) gives an upper bound of the traction force that can be generated by the kite. Thus, equation (18)-(21) can be employed to study the optimal operating conditions of the wing in order to compute an upper bound of the maximal generated power.

IV. Optimization of high-altitude wind energy generators

As described in Section III-B, the design of Kitenergy operational cycles involves several parameters that have to be set up according to the wind speed, the wing's characteristics, etc.. The optimal design of such parameters is hardly affordable in practice if the detailed model recalled in Section III-A is used, since it would be computationally very time-consuming. On the contrary, it can be quite easily carried out by employing the simplified equations presented in Section III-C. In this Section, such a procedure is employed to optimally design the operational cycles of a KE-yoyo and of a KE-carousel with either fixed or variable line length, in order to compare the energy generation potential of these systems.

A. Optimization of a KE-yoyo generator

As described in Section II-B, the operation of a KE-yoyo is divided into two phases, the traction and the passive ones. The operational parameters are the values θ_{trac} and θ_{pass} of angle θ during the traction and passive phase, the minimal cable length $\underline{r}$ during the cycle and the cable speed during the traction and the passive phase, $\dot{r}_{\text{trac}}$ and $\dot{r}_{\text{pass}}$ respectively.

By indicating with $P_{\text{trac}}(t)$ and $P_{\text{pass}}(t)$ the power generated (or spent) in the traction and passive phases respectively, the average power $\overline{P}$ obtained in a cycle can be computed as:

$$\overline{P} = \frac{\int_{t_0}^{t_{\text{trac,end}}} P_{\text{trac}}(\tau)d\tau + \int_{t_{\text{trac,end}}}^{t_{\text{pass,end}}} P_{\text{pass}}(\tau)d\tau}{t_{\text{pass,end}} - t_0} \tag{22}$$

where t_0 and $t_{\text{trac,end}}$ are the starting and ending instants of the traction phase and $t_{\text{pass,end}}$ is the ending instant of the passive phase (in this analysis, it is assumed that the starting instant of the passive phase coincides with the ending instant of the traction one). Assume that:

- approximately constant angles θ_{trac} and θ_{pass} during the traction and passive phases are kept, as well as constant ϕ angle;
- constant cable unrolling speed $\dot{r}_{\text{trac}} > 0$ and winding back speed $\dot{r}_{\text{pass}} < 0$ are employed during the traction and passive phases respectively;
- the amplitude Δr of the variation of the cable length r during each cycle is imposed and it is relatively small (e.g. 50 m) with respect to the minimal cable length $\underline{r}$, which occurs at the beginning of each traction phase.

The third assumption makes it possible to consider, with little approximation error, a unique length value $\underline{r}$ for the cables during the whole operational cycle and consequently, together with the assumptions on constant line speed and angles θ and ϕ, unique values $F_{\text{trac}}^{\text{c,trc}}$ and $F_{\text{pass}}^{\text{c,trc}}$ of the cable forces generated in the traction and in the passive phases respectively. Then, on the basis of the considered assumptions, a simplified formulation for the average power $\overline{P}$ is obtained:

$$\overline{P} = \frac{\left(F_{\text{trac}}^{\text{c,trc}}\dot{r}_{\text{trac}}(t_{\text{trac,end}} - t_0)\right) + \left(F_{\text{pass}}^{\text{c,trc}}\dot{r}_{\text{pass}}(t_{\text{pass,end}} - t_{\text{trac,end}})\right)}{t_{\text{pass,end}} - t_0} \tag{23}$$

Note that also equation (22) could be employed in the following analyses, e.g. using numerical integration, however the increase of accuracy with respect to the simplified equation (23) would be negligible. Now, by imposing a periodicity condition on the cable length r and considering the fixed cable length variation Δr, the time intervals $(t_{\text{trac,end}} - t_0)$ and $(t_{\text{pass,end}} - t_{\text{trac,end}})$ can be expressed as functions of $\dot{r}_{\text{trac}}$ and $\dot{r}_{\text{pass}}$ as follows (recalling that $\dot{r}_{\text{pass}} < 0$):

$$\begin{aligned} (t_{\text{trac,end}} - t_0) &= \frac{\Delta r}{\dot{r}_{\text{trac}}} \\ (t_{\text{pass,end}} - t_{\text{trac,end}}) &= \frac{-\Delta r}{\dot{r}_{\text{pass}}} \end{aligned} \tag{24}$$

On the basis of equations (23) and (24), through straightforward manipulations the following equation is obtained:

$$\overline{P} = \left(F_{\text{trac}}^{\text{c,trc}} - F_{\text{pass}}^{\text{c,trc}}\right)\frac{\dot{r}_{\text{trac}}\,\dot{r}_{\text{pass}}}{\dot{r}_{\text{pass}} - \dot{r}_{\text{trac}}} \tag{25}$$

Equation (25) can be used to optimally design the KE-yoyo operating parameters. Indeed, the values of the forces $F_{\text{trac}}^{\text{c,trc}}$ and $F_{\text{pass}}^{\text{c,trc}}$ depend on the parameters to be optimized, according to the simplified equations (18)-(21). If a wind profile is considered in equation (20) (e.g. the wind shear model introduced in Section III-A), then the generated power

depends on the line length r, according to (3) and (8). Furthermore, the coefficient C in (19) also depends on r, due to its influence on line drag. Thus, the traction force on the cable is computed as:

$$F^{\text{c,trc}}(\theta, \phi, \dot{r}, r) = C(r) \left(W_x(r \cos(\theta)) \sin(\theta) \cos(\phi) - \dot{r}\right)^2$$

It can be noted that the value of ϕ that gives the maximal traction force is $\phi^* = 0$, as it can be derived also by intuition since $\phi = 0$ means that the wing is flying perfectly downwind. Thus, the value $\phi = 0$ is chosen for the whole cycle. With the chosen value of ϕ, the cable forces during the traction and passive phases can be computed as:

$$\begin{array}{l} F^{\text{c,trc}}_{\text{trac}}(\theta_{\text{trac}}, \dot{r}_{\text{trac}}, \underline{r}) = \\ C_{\text{trac}}(r_{\text{trac}}) \left(W_x(\underline{r} \cos(\theta_{\text{trac}})) \sin(\theta_{\text{trac}}) - \dot{r}_{\text{trac}}\right)^2 \\ F^{\text{c,trc}}_{\text{pass}}(\theta_{\text{pass}}, \dot{r}_{\text{pass}}, \underline{r}) = \\ C_{\text{pass}}(r_{\text{pass}}) \left(W_x(\underline{r} \cos(\theta_{\text{pass}})) \sin(\theta_{\text{pass}}) - \dot{r}_{\text{pass}}\right)^2 \end{array} \tag{26}$$

where the values of C_{trac} and C_{pass} are computed according to (19), considering that different lift and drag coefficients have to be taken into account in the traction and in the passive phases, due to the low lift maneuver (as explained in Section II-B).
Therefore, the following optimization problem can be considered to design the operational parameters of the KE-yoyo:

$$\left(\theta^*_{\text{trac}}, \dot{r}^*_{\text{trac}}, \underline{r}^*, \theta^*_{\text{pass}}, \dot{r}^*_{\text{pass}}\right) = \arg\max \overline{P}\left(\theta_{\text{trac}}, \dot{r}_{\text{trac}}, \underline{r}, \theta_{\text{pass}}, \dot{r}_{\text{pass}}\right)$$

Furthermore, operational constraints have to be taken into account in the optimization, in order to find out feasible operating conditions. In particular, the involved constraints regard the maximal and minimal cable unrolling/rewinding speed, the minimal elevation of the wing from the ground (considering also its maneuvering radius, see Section II-A), the minimal angle θ during the cycle and the cable breaking force. The constraints on the line speed are the following:

$$\dot{r}_{\text{min}} \leq \dot{r} \leq \min(W_x(\underline{r} \cos(\theta)) \sin(\theta), \dot{r}_{\text{max}})$$

where $\dot{r}_{\text{min}}$, $\dot{r}_{\text{max}}$ are imposed by the limitations of the electric drives employed on the KSU and by the need to prevent excessive cable wear, due to the high unrolling/rewinding speed. Considering the maneuvering radius R_F (1) of the kite, a minimal elevation $\underline{Z}$ can be imposed by requiring that (see Fig. 13):

$$\underline{r} \cos\left(\theta + \tfrac{R_F}{\underline{r}+\Delta r}\right) \geq \underline{Z}$$

A constraint on the minimal value of θ is also introduced, in order to keep the wing trajectory contained in a relatively small area and to obtain short idle time intervals between the traction and recovery phases:

$$\theta \geq \underline{\theta}$$

with $0 \leq \underline{\theta} \leq \pi/2$. Finally, the constraint related to the cable breaking load can be expressed, for two cables with a given cable diameter d_l, as:

$$\begin{array}{l} F^{\text{c,trc}}_{\text{trac}} \leq 2 c_s \overline{F}(d_l) \\ F^{\text{c,trc}}_{\text{pass}} \leq 2 c_s \overline{F}(d_l) \end{array}$$

where $\overline{F}(\cdot)$ is the minimum breaking force of a single cable (see e.g. [15] for details) and c_s is a safety coefficient.

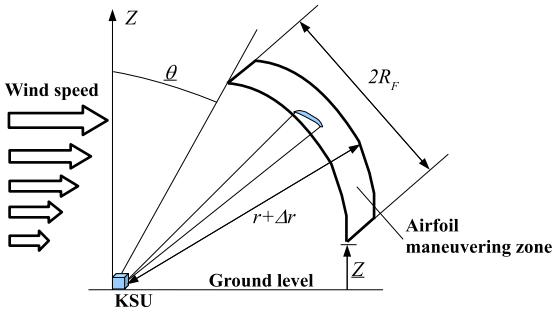

Fig. 13. KE-yoyo operation: constraints on minimal elevation Z and on minimal angle θ.

Considering all of the described constraints, the optimization problem to be solved is given by:

$$\begin{array}{c} \left(\theta^*_{\text{trac}}, \dot{r}^*_{\text{trac}}, \underline{r}^*, \theta^*_{\text{pass}}, \dot{r}^*_{\text{pass}}\right) = \\ \arg\max \overline{P}\left(\theta_{\text{trac}}, \dot{r}_{\text{trac}}, \underline{r}, \theta_{\text{pass}}, \dot{r}_{\text{pass}}\right) \\ \text{s. t.} \\ \dot{r}_{\text{min}} \leq \dot{r} \leq \min(W_x(\underline{r} \cos(\theta)) \sin(\theta), \dot{r}_{\text{max}}) \\ \underline{r} \cos\left(\theta + \tfrac{2 R_F}{2(\underline{r}+\Delta r)}\right) \geq \underline{Z} \\ \theta \geq \underline{\theta} \\ F^{\text{c,trc}}_{\text{trac}} \leq 2 c_s \overline{F}(d_l) \\ F^{\text{c,trc}}_{\text{pass}} \leq 2 c_s \overline{F}(d_l) \end{array} \tag{27}$$

Using the system data given in Table III and the wind shear profile reported in Fig. 10, the solution of the optimization problem (27) is the following:

$$\begin{pmatrix} \theta^*_{\text{trac}} \\ \dot{r}^*_{\text{trac}} \\ \underline{r}^* \\ \theta^*_{\text{pass}} \\ \dot{r}^*_{\text{pass}} \end{pmatrix} = \begin{pmatrix} 69.1^\circ \\ 2.14\,\text{m/s} \\ 631\,\text{m} \\ 50^\circ \\ -6.0\,\text{m/s} \end{pmatrix} \tag{28}$$

The course of the power obtained by means of simplified equations is shown in Fig. 14. The corresponding optimal average power value is equal to 2.2 MW.

TABLE III
OPTIMIZATION OF A KE-YOYO OPERATIONAL CYCLE WITH LOW LIFT MANEUVER: SYSTEM PARAMETERS

A	500 m^2	Characteristic area
d_l	0.04 m	Diameter of a single line
$\overline{F}(d_l)$	1.50 10^6 N	Minimum breaking load of a single line
C_L	1.3	Average kite lift coefficient - traction phase
E	12.5	Average kite efficiency - traction phase
$C_{L,WG}$	0.1	Kite lift coefficient - low lift maneuver
$C_{D,WG}$	0.5	Kite drag coefficient - low lift maneuver
$C_{D,l}$	1	Line drag coefficient
ρ	1.2 kg/m^3	Air density
Δr	50 m	Maximum line variation during a cycle
$\dot{r}_{\text{min}}$	-6.0 m/s	Minimal line speed
$\dot{r}_{\text{max}}$	6 m/s	Maximal line speed
$\underline{Z}$	30 m	Minimal elevation from the ground
$\underline{\theta}$	50	Minimal angle θ
c_s	2	Safety coefficient
w_s	80 m	wing wingspan

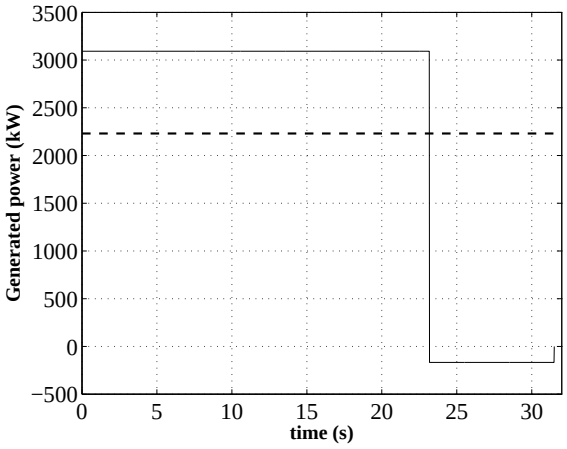

Fig. 14. Optimized operation of a KE-yoyo with low lift maneuver in one complete cycle, computed using the simplified power equations. Mean (dashed) and actual (solid) generated power.

B. Optimization of a KE-carousel generator with constant cable length and vehicle speed

In the KE-carousel with constant cable length, power is generated by the vehicle movement. The line rolling speed $\dot{r}$ is equal to zero, while the tangential speed $R\dot{\Theta}$ is kept constant. Thus, the angular acceleration $\ddot{\Theta}$ is zero and, from (7), the force F^{gen} is:

$$F^{\text{gen}} = F^{\text{c,trc}} \sin(\theta) \sin(\phi).$$

Besides, from (21) and since $\dot{r} = 0$, the generated power $P^{\text{const}}_{\text{KE-carousel}}$ is

$$\begin{aligned} P^{\text{const}}_{\text{KE-carousel}} &= F^{\text{gen}} R\dot{\Theta} \\ &= F^{\text{c,trc}} \sin(\theta) \sin(\phi) R\dot{\Theta} \end{aligned} \tag{29}$$

By combining equations (18), (20) and (29), the following expression of $P_{\text{KE-carousel}}$ is obtained:

$$P^{\text{const}}_{\text{KE-carousel}} = C \left| \vec{W}_{e,r} \right|^2 \sin(\theta) \sin(\phi) R\dot{\Theta}$$

where

$$\left| \vec{W}_{e,r} \right| = \left| \sin(\theta) \left(W_x (r \cos\theta) \cos(\Theta + \phi) - R\dot{\Theta} \sin(\phi) \right) \right|.$$

The instantaneous generated power $P^{\text{const}}_{\text{KE-carousel}}$ depends on the KE-carousel angular position Θ. The mean power $\bar{P}^{\text{const}}_{\text{KE-carousel}}$ generated during the whole cycle can be computed as:

$$\bar{P}^{\text{const}}_{\text{KE-carousel}} = \frac{1}{t_{\text{end,cr}}} \int_0^{t_{\text{end,cr}}} P^{\text{const}}_{\text{KE-carousel}} \left(\Theta(t) \right) \mathrm{d}t \tag{30}$$

where $\Theta(0) = 0$ and $t_{\text{end,cr}}$ is the final time of the carousel cycle, i.e. $\Theta(t_{\text{end,cr}}) = 2\pi$. Since the angular velocity $\dot{\Theta}$ is constant, the angular position can be expressed as $\Theta(t) = \dot{\Theta} t$ and equation (30) can be written as

$$\bar{P}_{\text{KE-carousel}} = \frac{1}{2\pi} = \int_0^{2\pi} P_{\text{KE-carousel}} \left(\Theta \right) \mathrm{d}\Theta \tag{31}$$

As discussed in the KE-yoyo analysis (see Section IV-A), a minimum elevation $\underline{Z}$ of the kite during its flight is imposed by requiring that:

$$r \cos\left(\theta + \frac{R_F}{r} \right) \geq \underline{Z}$$

Moreover, the constraint related to the cable breaking load is expressed, for two cables with a given diameter d_l, as:

$$F^{\text{c,trc}} \leq 2 c_s \bar{F}(d_l)$$

where c_s is a safety coefficient and $\bar{F}(d_l)$ is the minimum breaking load of a single d_l-diameter cable.

In order to maximize numerically the average power (30), the carousel angular position range $[0, 2\pi]$ has been quantized by means of a uniform gridding with N samples Θ_i, with $i = 1, \ldots, N$. This a way, the mean power $\bar{P}^{\text{const}}_{\text{KE-carousel}}$ (30) can be approximated as

$$\bar{P}^{\text{const}}_{\text{KE-carousel}} = \frac{1}{N} \sum_{i=1}^{N} P_{\text{KE-carousel}} \left(\Theta_i \right) \tag{32}$$

and an approximation of the maximum mean generated power is computed as

$$\bar{P}^{\text{const}*}_{\text{KE-carousel}} = \max_{\substack{r,\, \dot{\Theta},\, \theta_i,\, \phi_i \\ i\,=\,1,\,\ldots\,,\,N}} \frac{1}{N} \sum_{i=1}^{\text{const},N} P_{\text{KE-carousel}} \left(r, \dot{\Theta}, \theta_i, \phi_i, \Theta_i \right) \tag{33a}$$

s. t.

$$\theta_i \geq 0 \quad i = 1, \ldots, N \tag{33b}$$

$$F^{\text{c,trc}}_i \leq 2 c_s \bar{F}(d_l) \quad i = 1, \ldots, N \tag{33c}$$

$$r \cos\left(\theta_i + \frac{5 w_s}{2r} \right) \geq \underline{Z} \quad i = 1, \ldots, N \tag{33d}$$

$$\sin(\theta) \left(W_x \cos(\Theta_i + \phi_i) - R\dot{\Theta} \sin(\phi_i) \right) \geq 0 \quad i = 1, \ldots, N \tag{33e}$$

where θ_i and ϕ_i are the values of the angles θ and ϕ at the carousel angular position Θ_i and $F^{\text{c,trc}}_i$ is the related traction force acting on the cables. The constraint (33e) has been included in order to ensure that the kite exerts a positive traction force on the cables.

Using the system data reported in Table IV and the wind shear profile reported in Fig. 10, the optimal vehicle tangential velocity $R\dot{\Theta}^*$ and optimal cable length r^* are:

$$\begin{pmatrix} R\dot{\Theta}^* \\ r^* \end{pmatrix} = \begin{pmatrix} 3.98 \text{ m/s} \\ 375 \text{ m} \end{pmatrix}, \tag{34}$$

while the optimal trajectories of the angles θ and ϕ (as function of the KE-carousel angular position Θ) are reported in Figs. 15(a) and 15(b), respectively. The optimal mean generated power $\bar{P}^{\text{const}*}_{\text{KE-carousel}}$ is equal to 1.89 MW. The values of the corresponding instantaneous generated power $P^{\text{const}}_{\text{KE-carousel}}$ as function of the angle Θ is reported in Fig. 16. As it can be seen in Fig. 15(a), for angular position Θ between 35° and 110° (corresponding to the passive phase), the generated power is zero, since the kite is at the border of the "power zone" (see Fig. 6). As a matter of fact, the angle θ is equal to zero, leading to a traction force on the cables $F^{\text{c,trc}}$ equal to zero. This means that, in this phase, the kite is not

TABLE IV

MODEL PARAMETERS EMPLOYED TO COMPUTE AN OPTIMAL KE-CAROUSEL CYCLE WITH CONSTANT CABLE LENGTH

A	500 m^2	Characteristic area
R	300 m	KE-carousel radius
C_L	1.3	Average kite lift coefficient
E	12.5	Average kite efficiency
d_l	0.04 m	Diameter of a single line
$C_{D,l}$	1	Line drag coefficient
ρ	1.2 kg/m^3	Air density
$\underline{Z}$	30 m	Minimal elevation from the ground
c_s	2	Safety coefficient
w_s	80 m	wing wingspan

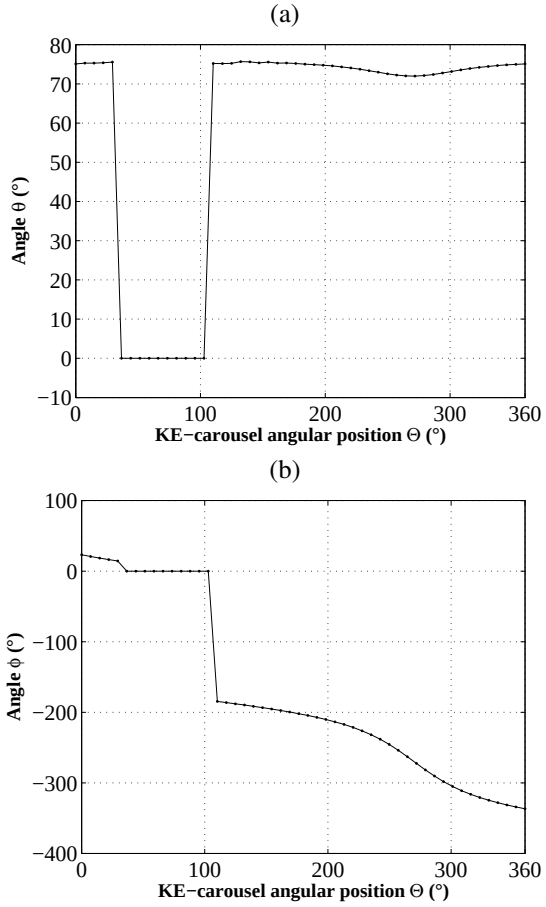

Fig. 15. Optimized operation conditions of a KE-carousel with constant cable length, computed using the simplified power equations. (a) angle θ and (b) angle ϕ during the whole KE-carousel cycle.

exerting any force in the direction of the vehicle longitudinal velocity, so that no power is generated or dissipated. On the other hand, in the traction phase the angle θ is about 75° and the angle ϕ is such that the kite pulls the vehicle, thus generating energy.

C. Optimization of a KE-carousel generator with variable cable length and vehicle speed

In this Section the third of the questions posed above is investigated, i.e. if it is possible to have a KE-carousel configuration that does not require passive phases, so that

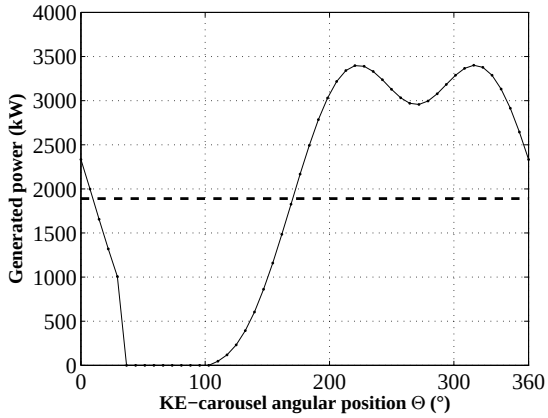

Fig. 16. Optimized operation conditions of a KE-carousel with constant cable length, computed using the simplified power equations. Mean (dashed) and actual (solid) generated power.

the energy production is constant and at its possible maximum. In order to simplify the analysis, in this section it is considered that the absolute wind speed $\vec{W}_0$ (introduced in Section III-A) is independent on elevation and it is parallel with respect to the ground. Under such assumptions, it can be shown that in the two previous KE configurations, the maximal power that can be obtained using the simplified equations is:

$$\max_t P(t) = C\frac{4}{27}|\vec{W}_0|^3 \tag{35}$$

However, the mean power is lower, since in the course of time lower values are obtained.

In this Section, the variable length KE-carousel operation will be analytically optimized. In particular, it will be shown that, by imposing suitable periodic courses of the carousel velocity and line unrolling speed, the theoretical upper bound of generated power (35) can be obtained continuously on average. In order to simplify the analysis, it is considered that the diameter of the two cables linking the wing to the KSU is fixed and that it is sufficiently high to make the cables able to support the generated traction forces. Moreover, the vehicle longitudinal acceleration is supposed to be negligible (see equation (7) in Section III-A), so that the following equation is obtained:

$$\begin{aligned} P^{\text{var}}_{\text{KE-carousel}} = F^{\text{c,trc}}\dot{r} + \dot{\Theta}\, R\, F^{\text{gen}}(t) = \\ F^{\text{c,trc}}\left(\dot{r} + R\,\dot{\Theta}\sin\theta\sin\phi\right) = \\ C|\vec{W}_{e,r}|^2\left(\dot{r} + R\,\dot{\Theta}\sin\theta\sin\phi\right) \end{aligned}$$

Thus, the overall power generated by a KE-carousel can be computed as:

$$\begin{aligned} &P^{\text{var}}_{\text{KE-carousel}} = \\ &C\left(\sin(\theta)\left(|\vec{W}_0|\cos(\Theta+\phi) - R\,\dot{\Theta}\sin(\phi)\right) - \dot{r}\right)^2 \\ &\left(\dot{r} + R\,\dot{\Theta}\sin\theta\sin\phi\right) \end{aligned} \tag{36}$$

For given values of angular position Θ and tangential speed $R\,\dot{\Theta}$, it is possible to compute the maximal overall power as

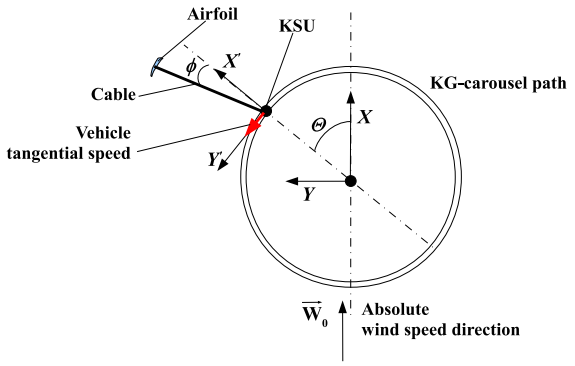

Fig. 17. Sketch of KE-carousel (top view).

follows:

$$P^{*\text{var}}_{\text{KE-carousel}}(\Theta,\dot{\Theta}) = \max_{\theta,\phi,\dot{r}} P^{\text{var}}_{\text{KE-carousel}}$$
$$\text{s. t.} \tag{37}$$
$$\dot{r} \leq \sin(\theta)\left(|\vec{W}_0|\cos(\Theta+\phi) - R\,\dot{\Theta}\sin(\phi)\right)$$

The constraint on $\dot{r}$ has been included in order to ensure that the kite exerts a positive traction force on the cables. The optimizer $(\theta^*, \phi^*, \dot{r}^*)^T$ can be analytically computed as:

$$\begin{pmatrix} \theta^* \\ \phi^* \\ \dot{r}^* \end{pmatrix} = \begin{pmatrix} \frac{\pi}{2} \\ -\Theta \\ \frac{|\vec{W}_0|}{3} + R\,\dot{\Theta}\sin(\Theta) \end{pmatrix} \tag{38}$$

By replacing the optimal values (38) in equation (36) the following maximal power value is obtained:

$$P^{*\text{var}}_{\text{KE-carousel}}(\Theta,\dot{\Theta}) = \frac{4}{27}C|\vec{W}_0|^3 \tag{39}$$

Thus, according to result (39), in any KE-carousel operating condition (in terms of Θ and $\dot{\Theta}$) the constant value (39) of the generated power can be achieved by choosing ϕ and $\dot{r}$ given in (38). Now, an optimal KE-carousel operating cycle can be designed by choosing a suitable course of the vehicle angular speed $\dot{\Theta}$, such that a periodic course of all the involved variables is achieved. In particular, it is needed that the average value of $\dot{r}$ over a complete cycle equals zero:

$$\frac{1}{2\pi}\int_0^{2\pi} (\dot{r}(\Theta))\,d\Theta = 0 \tag{40}$$

By considering a periodical course of $R\,\dot{\Theta}$ of the form:

$$R\,\dot{\Theta} = R\,\overline{\dot{\Theta}}(1-\sin(\Theta)) \tag{41}$$

and imposing the optimal value $\dot{r}^*$ (38) of $\dot{r}$, the following result is obtained for $\overline{\dot{\Theta}}$:

$$\dot{r} = \tfrac{|\vec{W}_0|}{3} + R\,\overline{\dot{\Theta}}(1-\sin(\Theta))\sin(\Theta)\tfrac{1}{2\pi}\int_0^{2\pi}(\dot{r}(\Theta))\,d\Theta =$$
$$= \tfrac{|\vec{W}_0|}{3} - R\,\overline{\dot{\Theta}}\tfrac{1}{2\pi}\int_0^{2\pi}\left(\sin(\Theta)^2\right)d\Theta = \tfrac{|\vec{W}_0|}{3} - \tfrac{1}{2}R\,\overline{\dot{\Theta}}$$

$$\Rightarrow R\,\overline{\dot{\Theta}} = \frac{2}{3}|\vec{W}_0| \tag{42}$$

From (41) and (42) the following course for the angular speed $\dot{\Theta}$ is obtained:

$$R\,\dot{\Theta} = \frac{2}{3}|\vec{W}_0|(1-\sin(\Theta)) \tag{43}$$

The optimal courses of $\dot{\Theta}$, $\dot{r}$ and of the power P_{vehicle}, P_{line} generated by the vehicle motion and by the line unrolling respectively, as well as the overall optimal power $P^*_{\text{KE-carousel}}$, are reported in Fig. 18(a)-(b) as functions of the vehicle angular position Θ. The considered KE-carousel characteristics are reported in Table V. The overall power is constant and

TABLE V
MODEL PARAMETERS EMPLOYED TO COMPUTE AN OPTIMAL KE-CAROUSEL CYCLE

A	500 m^2	Characteristic area
r	600 m	Mean line length
R	300 m	KE-carousel radius
C_L	1.3	wing lift coefficient
E	12.5	Aerodynamic efficiency
d_l	0.04 m	Diameter of a single line
$C_{D,l}$	1	Line drag coefficient
ρ	1.2 kg/m^3	Air density
$\lvert\vec{W}_0\rvert$	8.3 m/s	Nominal wind speed magnitude

equal to $\frac{4}{27}C|\vec{W}_0|^3 = 3.4\,\text{MW}$, i.e. the maximal power is continuously obtained. Note that the wind conditions in Table V approximately corresponds to the average wind at the kite altitude in the optimized KE-yoyo and constant-cable KE-carousel presented in Sections IV-A-IV-B, whose average power values were 2.2 MW and 1.89 MW respectively. As it can be noted in Fig. 18(a), the optimal cycle is such that $\dot{\Theta} = 0$ when $\Theta = \pi/2$, meaning that the vehicle should stop at such an angular position. This would prevent the KE-carousel from completing the cycle, however such issue could be easily solved by slightly modifying the optimal course of $\dot{\Theta}$.

V. SIMULATION RESULTS

In order to assess the control system performance and the matching between simplified equations and dynamical model of the system, numerical simulations of the KE-yoyo and of the constant-line KE-carousel have been performed. In Fig. 19(a) the kite aerodynamical coefficients C_L and C_D employed during the simulation are reported, while the related aerodynamic efficiency E is shown in Fig. 19(b). The wind shear profile (3) with $Z_0 = 32.5\,\text{m}$, $W_0 = 7.4\,\text{m/s}$ and $Z_r = 6\,10^{-4}\,\text{m}$ (corresponding to the wind profile in Fig. 10) has been used during the simulation. Furthermore, in order to better evaluate the matching between the results obtained through simplified equations and numerical simulation, the latter has been performed with no wind disturbances.

A. KE-yoyo simulation

The model and control parameters employed in the simulation of the KE-yoyo are reported in Table VI. The optimal values $\underline{r}^* = 631$ m, $\dot{r}^*_{\text{trac}} = 2.14$ m/s, and $\dot{r}^*_{\text{pass}} = -6$ m/s computed solving optimization problems (27) have been employed as parameters in the numerical simulation. The

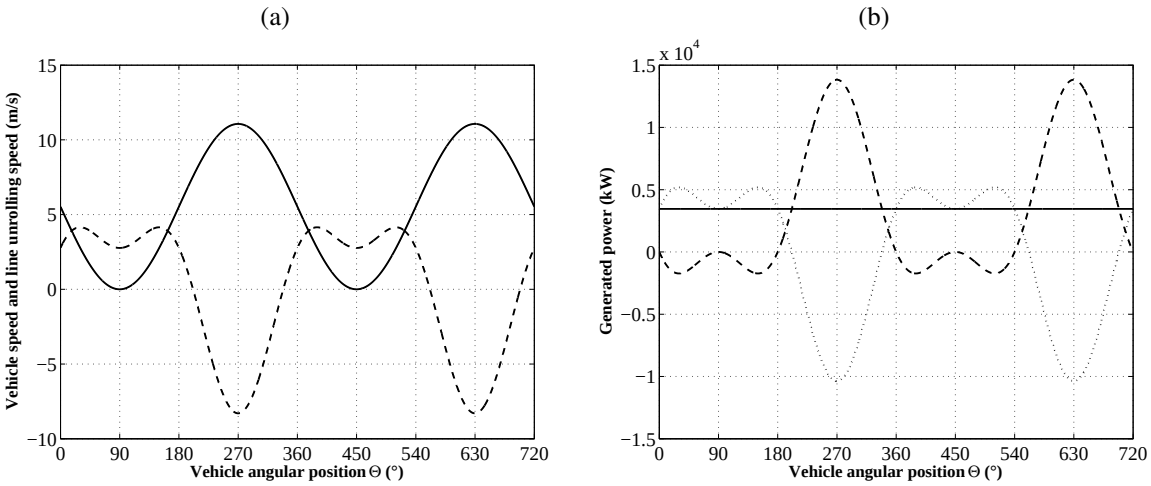

Fig. 18. (a) Line speed $\dot{r}$ (dashed) and vehicle speed $R\dot{\Theta}$ (solid) during two complete optimal KE-carousel cycles as functions of Θ. (b) Power P_{vehicle} generated by the vehicle motion (dash-dot), power P_{line} given by the line unrolling (dashed) and overall optimal power $P^*_{\text{KE-carousel}}$ (solid).

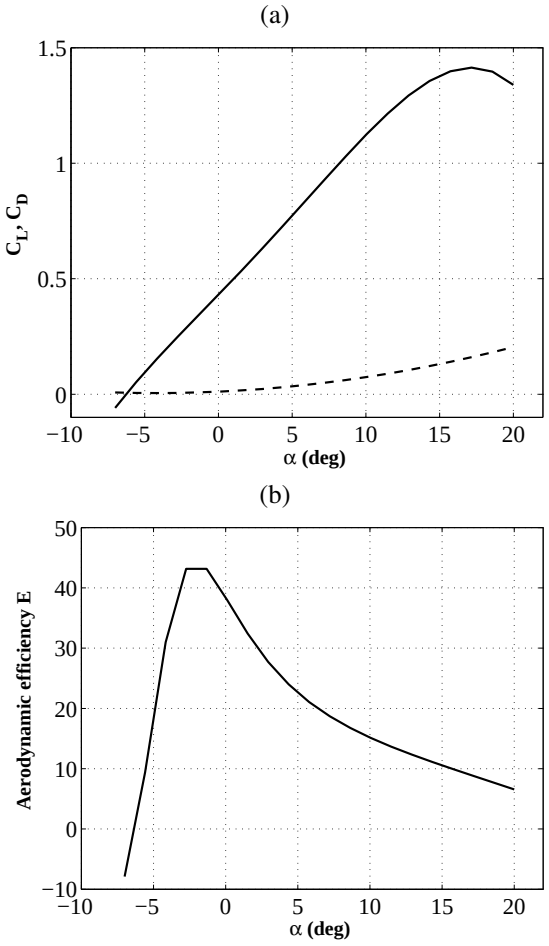

Fig. 19. (a) Kite lift coefficient C_L (solid) and drag coefficient C_D (dashed) as functions of the angle of attack α. (b) Aerodynamic efficiency E as function of the attack angle α.

TABLE VI

NUMERICAL SIMULATION OF A KE-YOYO WITH OPTIMIZED OPERATIONAL CYCLE: SYSTEM AND CONTROL PARAMETERS.

m	300 kg	Kite mass
A	500 m^2	Characteristic area
d_l	0.04 m	Diameter of a single line
ρ_l	970 kg/m^3	Line density
$C_{D,l}$	1	Line drag coefficient
α_0	3.5°	Base angle of attack
ρ	1.2 kg/m^3	Air density
Δr	50 m	Maximum line variation during a cycle
θ_I	55°	Traction phase starting conditions
ϕ_I	45°	
$\underline{r}$	631 m	
$\overline{r}$	681 m	Passive phase starting condition
$\overline{\theta}_{III}$	50°	Wing glide starting condition
$\overline{\psi}$	6°	Input constraints
$\overline{\dot{\psi}}$	20°/s	
$\dot{r}_{\text{trac}}$	2.14 m/s	Traction phase reference $\dot{r}_{\text{ref}}$
$\dot{r}_{\text{pass}}$	-6.0 m/s	Passive phase reference $\dot{r}_{\text{ref}}$
T_c	0.2 s	Sample time
N_c	1 step	Control horizon
N_p	10 steps	Prediction horizon

results related to a complete cycle are presented. The obtained kite trajectory is reported in Fig. 20. It can be noted that during the traction phase the kite follows "figure eight" orbits and that its elevation Z goes from about 214 m to 389 m, corresponding to a mean value of $\theta(t)$ equal to 68°, consistently with the optimized value (28), while the lateral angle $\phi(t)$ oscillates between $\pm 10°$ with zero in average. The power generated in the simulation is reported in Fig. 21 and compared with the optimal power course computed using the simplified equations: the mean value is 1.75 MW, thus showing an error of about 20% with respect to the optimal value (2.2 MW), due to the presence of the inertial and apparent forces, the cable weight and the idle time between the traction and passive phases. In fact, such aspects are not taken into account in the simplified equations. Finally, the course of the kite attack angle is reported in Fig. 22.

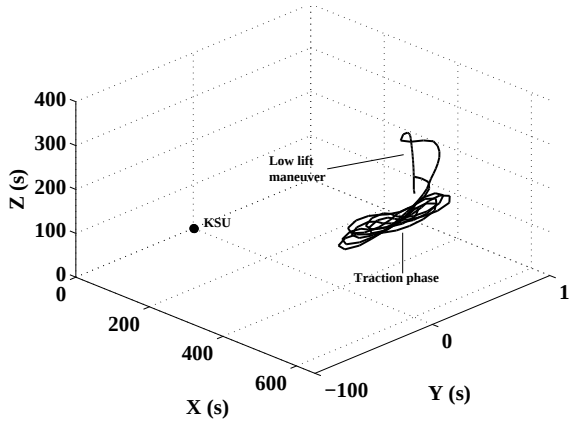

Fig. 20. Optimized operation of a KE-yoyo with low lift maneuver: kite trajectory during one complete cycle.

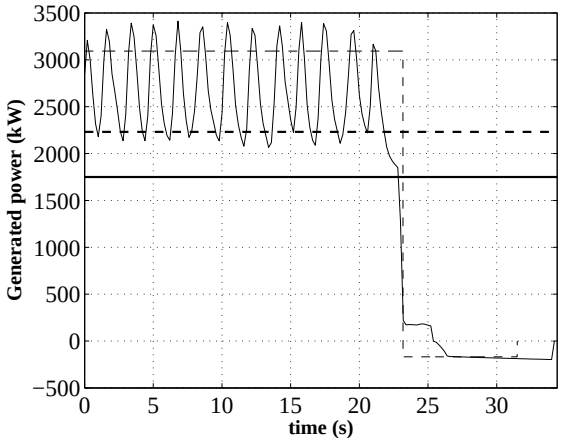

Fig. 21. Optimized operation of a KE-yoyo with low lift maneuver in one complete cycle. Instantaneous generated power by means of simplified equations (dashed thin line) and by numerical simulation (solid thin line). Average generated power by means of simplified equations (dashed thick line) and by numerical simulation (solid thick line).

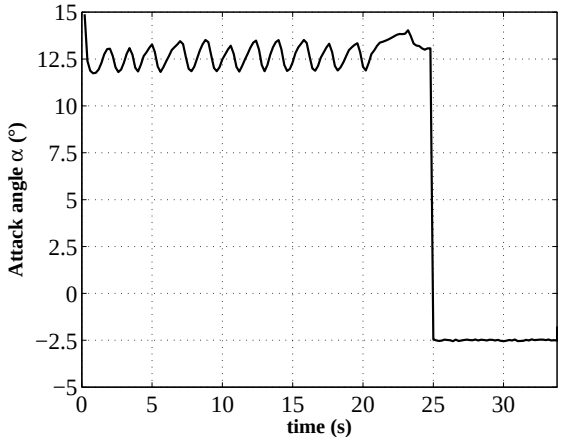

Fig. 22. Optimized operation of a KE-yoyo with low lift maneuver: Angle of attack during one complete cycle simulated using the detailed nonlinear system model and NMPC controller.

B. KE-carousel simulation with constant cable length

The numerical simulation of the constant-cable KE-carousel has been performed employing the optimal parameters $r^* = 375$ m and $R\dot{\Theta}^* = 3.98$ m/s, according to (34). Furthermore, the system and control parameters used in the simulation are reported in Table VII. The results related to one complete cycle of the KE-carousel are presented. In particular, the obtained kite trajectory is shown in Fig. 23, while the courses of the angle $\theta(t)$ and $\phi(t)$, together with the optimal values θ_i^* and ϕ_i^* which solve (33) exploiting the simplified equations, are reported in Figs. 24(a) and 24(b) respectively. A comparison between the generated power

TABLE VII

NUMERICAL SIMULATION OF A KE-CAROUSEL WITH OPTIMIZED OPERATIONAL CYCLE: SYSTEM AND CONTROL PARAMETERS.

m	300 kg	Kite mass
A	500 m^2	Characteristic area
R	300 m	KE-carousel radius
d_l	0.04 m	Diameter of a single line
ρ_l	970 kg/m^3	Line density
$C_{D,l}$	1	Line drag coefficient
α_0	3.5°	Base angle of attack
ρ	1.2 kg/m^3	Air density
r	335 m	Line length
$R\dot{\Theta}$	3.9 m/s	Vehicle longitudinal velocity
$\overline{\psi}$	6°	Input constraints
$\overline{\dot{\psi}}$	20°/s	
T_c	0.2 s	Sample time
N_c	1 step	Control horizon
N_p	10 steps	Prediction horizon

obtained in the simulation and the corresponding optimal result obtained solving (33), is reported in Fig. 25. The mean generated power obtained in the simulation is 1.78 MW, thus showing an error of about 5% with respect to the optimal value (1.89 MW) obtained solving (33). Finally, the course of the angle of attack is reported in Fig. 26.

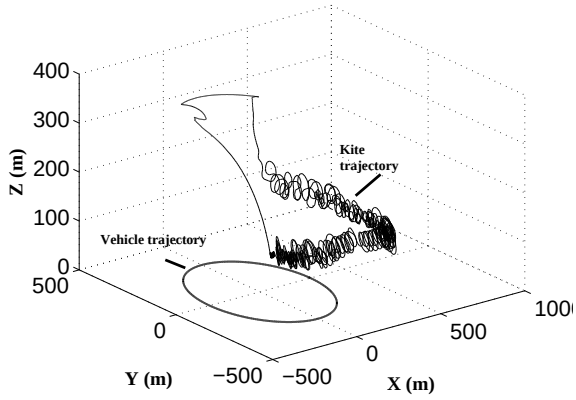

Fig. 23. Optimized operation conditions of a KE-carousel with constant cable length. Vehicle and kite trajectories during one complete cycle simulated using the detailed nonlinear system model and NMPC controller..

VI. CONCLUSIONS

The paper presented an overview of the innovative Kitenergy technology which, by exploiting controlled tethered wings to extract energy from high-altitude wind, has the potential to provide large quantities of renewable energy

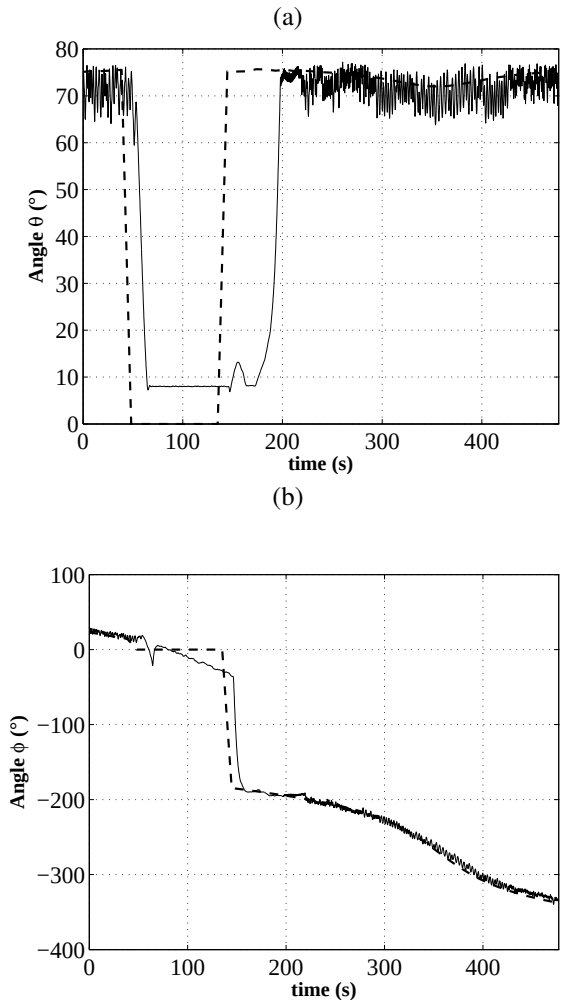

Fig. 24. Optimized operation of a constant-cable KE-carousel during one cycle, simulated using the detailed nonlinear system model and NMPC controller. (a) Angle θ in the numerical simulation (solid) and using simplified equations (dashed). (b) Angle ϕ in the numerical simulation (solid) and using simplified equations (dashed).

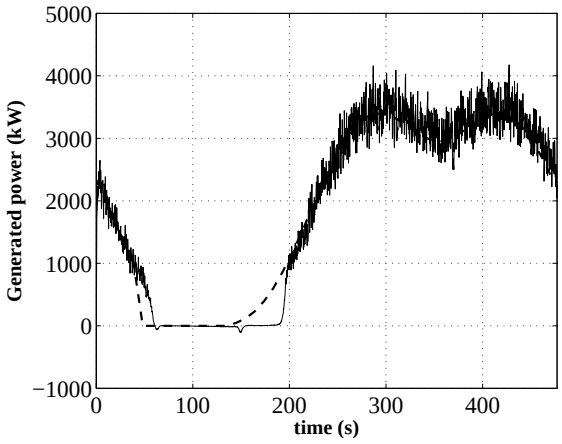

Fig. 25. Optimized operation of a constant-cable KE-carousel during one cycle, simulated using the detailed nonlinear system model and NMPC controller. Course of the generated power (solid line) and comparison with the optimized course obtained using the simplified equations (dashed).

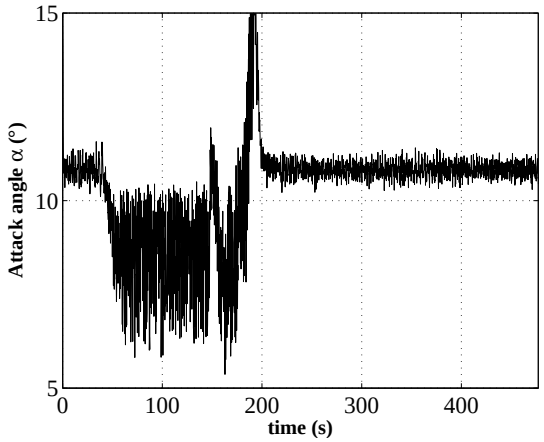

Fig. 26. Optimized operation of a KE-carousel with constant cable during one cycle, simulated using the detailed nonlinear system model and NMPC controller: course of the angle of attack α during one complete cycle.

at lower cost than fossil energy, thus realizing a radical shift in the energy scenario. As a novel contribution with respect to previous works, the operational cycles of Kitenergy generators have been optimized by using simplified power equations, in order to evaluate the maximal power that can be generated. Finally, simulations with a detailed system model have been carried out to test the optimized operational cycles and to assess the performance of the employed control strategy, based on NMPC. The simulation results showed that the designed controller is able to achieve optimal power performance, while satisfying operational constraints, thus confirming the results obtained so far regarding the energy generation potentials of Kitenergy technology. Moreover, the reported analyses allow to carry out a more complete comparison between the considered Kitenergy configurations. In particular, with the considered wing and wind characteristics, similar average power values of about 1.8 MW have been obtained with the KE-yoyo and with the constant-cable KE-carousel configurations. It can be noted that the maximal values of the instantaneous generated power in these configurations are about 3.2 MW and 3.3 MW respectively. Thus, the rated power of the generators equipped on the KSU (for the KE-yoyo) and on the vehicle (for the KE-carousel with constant cable) have to be about 3.2 MW and 3.3 MW respectively (i.e. about twice the mean generated power). These two configurations have similar power generation characteristics but also very different operational cycles, that lead to diverse advantages and potential problems. In fact, being the KSU fixed on the ground, a KE-yoyo is less complex and expensive to build than a constant-cable KE-carousel, however it may have problems related to excessive cable wear due to line rolling/unrolling under high traction forces. The latter problem is avoided by the KE-carousel with constant cable length. As regards the variable cable KE-carousel, it has been shown in this paper that the maximal overall power can be continuously generated with this configuration, without passive phases. In particular, a power of about 3.4 MW has been obtained in the considered conditions, i.e.

about 60-80% higher than the average power achieved by the other configurations. However, in the variable-cable KE-carousel the rated power of the generators equipped on the vehicle has to be about 15 MW (i.e. four times the obtained net power), while the KSU has to be able to provide about 10 MW to recover the wing in the traction phase. Thus, the advantages of larger and more constant power generation with respect to the other KE configurations are paid in terms of larger costs for the electric equipments and the mechanical structure and of greater construction complexity of the variable length KE-carousel. These results will be important in the next steps of the project, where the tradeoff among these different features has to be assessed to select the "best" configuration to be used for the development of an industrial generator prototype.

REFERENCES

[1] International Energy Agency (IEA), *World Energy Outlook 2009*. Paris, France: IEA PUBLICATIONS, 2009.

[2] U. S. Energy Information Administration (EIA), "International Energy Outlook 2009," May 2009, available online: http://www.eia.doe.gov/oiaf/ieo/index.html.

[3] "Global wind energy council, *Global wind 2007 report*," May 2008, available online: http://www.gwec.net/fileadmin/documents/test2/gwec-08-update_FINAL.pdf.

[4] C. L. Archer and M. Z. Jacobson, "Evaluation of global wind power," *J. Geophys. Res.*, vol. 110, D12110, 2005.

[5] G. M. Masters, *Renewable and Efficient Electric Power Systems*. Wiley, 2004.

[6] R. Thresher, M. Robinson, and P. Veers, "To capture the wind," *IEEE Power & Energy Magazine*, vol. 5, no. 6, pp. 34–46, 2007.

[7] C. L. Archer and K. Caldeira, "Global assessment of high-altitude wind power," *Energies*, vol. 2, no. 2, pp. 307–319, 2009.

[8] M. S. Manalis, "Airborne windmills and communication aerostats," *Journal of Aircraft*, vol. 13, no. 7, pp. 543–544, 1976.

[9] C. A. J. Fletcher and B. W. Roberts, "Electricity generation from jet-streams winds," *Journal of Energy*, vol. 3, pp. 241–249, 1979.

[10] M. L. Loyd, "Crosswind kite power," *Journal of Energy*, vol. 4, no. 3, pp. 106–111, 1980.

[11] W. J. Ockels, "Laddermill, a novel concept to exploit the energy in the airspace," *Aircraft Design*, vol. 4, no. 2, pp. 81–97, 2001.

[12] P. Williams, B. Lansdorp, and W. Ockels, "Optimal crosswind towing and power generation with tethered kites," *Journal of guidance, control, and dynamics*, vol. 31, pp. 81–93, 2008.

[13] M. Canale, L. Fagiano, and M. Milanese, "Power kites for wind energy generation," *IEEE Control Systems Magazine*, vol. 27, no. 6, pp. 25–38, December 2007.

[14] ——, "High altitude wind energy generation using controlled power kites," *IEEE Transactions on Control Systems Technology*, vol. 18, no. 2, pp. 279–293, 2010, doi: 10.1109/TCST.2009.2017933.

[15] L. Fagiano, M. Milanese, and D. Piga, "High-altitude wind power generation," *IEEE Transactions on Energy Conversion*, vol. 25, no. 1, pp. 168–180, 2010, doi: 10.1109/TEC.2009.2032582.

[16] A. Ilzhöfer, B. Houska, and M. Diehl, "Nonlinear MPC of kites under varying wind conditions for a new class of large-scale wind power generators," *International Journal of Robust and Nonlinear Control*, vol. 17, pp. 1590–1599, 2007.

[17] Sky Wind Power Corporation, http://www.skywindpower.com.

[18] Magenn Power Inc., http://www.magenn.com.

[19] Makani Power Inc., http://www.makanipower.com.

[20] Joby Energy Inc., http://www.jobyenergy.com.

[21] SkyMill Energy Inc., http://www.skymillenergy.com.

[22] SkySails GmbH & Co., http://www.skysails.info.

[23] KiteNav project website, http://www.kitenav.com.

[24] L. Fagiano, M. Milanese, V. Razza, and I. Gerlero, "Offshore high-altitude wind energy using controlled airfoils," in *European Wind Energy Conference (EWEC) 2010*, Warsaw, PL, 2010.

[25] Vestas Wind Systems A/S, "Vestas v90 brochure," available online: http://www.vestas.com.

[26] L. Fagiano, "Control of tethered airfoils for high–altitude wind energy generation," Ph.D. dissertation, Politecnico di Torino, Italy, February 2009, available on–line: http://lorenzofagiano.altervista.org/docs/PhD_thesis_Fagiano_Final.pdf.

[27] National Oceanic & Atmospheric Administration – Earth System Research Laboratory, NOAA/ESRL Radiosonde Database Access: http://raob.fsl.noaa.gov/.

[28] D. Q. Mayne, J. B. Rawlings, C. V. Rao, and P. Scokaert, "Constrained model predictive control: Stability and optimality," *Automatica*, vol. 36, pp. 789–814, 2000.

[29] M. Canale, L. Fagiano, and M. Milanese, "Set Membership approximation theory for fast implementation of model predictive control laws," *Automatica*, vol. 45, no. 1, pp. 45–54, 2009.

[30] M. Milanese, C. Novara, K. Hsu, and K. Poolla, "The filter design from data (fd2) problem: Nonlinear set membership approach," *Automatica*, vol. 45, no. 10, pp. 2350–2357, 2009.

[31] International Energy Agency (IEA), *Projected Cost of Generating Energy – 2005 update*. Paris, France: IEA PUBLICATIONS, 2008, available on–line: http://www.iea.org/Textbase/publications/free_new_Desc.asp?PUBS_ID=1472.

[32] Kitenergy project, experimental test movie (2008, Jan.), [Online]. Available on–line: http://lorenzofagiano.altervista.org/movies/Casale_test.wmv.

[33] Kitenergy project, experimental test movie (2006, Aug.), [Online]. Available: http://lorenzofagiano.altervista.org/movies/Sardinia_test.wmv.

[34] B. Houska, "Robustness and stability optimization of open-loop controlled power generating kites," Master's thesis, University of Heidelberg, 2007.

[35] D. Piga, "Analisi delle prestazioni del sistema kitegen: eolico di alta quota," Master's thesis, Politecnico di Torino, 2008, (in Italian).